

Formation of Organized Protein Thin Films with External Electric Field

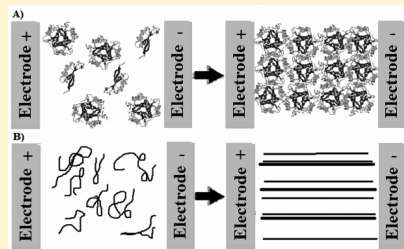
Cecília Fabiana da G. Ferreira* and Paulo C. Camargo[†]

PIPE, Federal University of Paraná, Centro Politécnico - Adm. Building, 2° Floor, 81531-990 Curitiba, Paraná, Brazil

Elaine M. Benelli

Biochemistry and Molecular Biology, Federal University of Paraná, P.O. Box 19046, 81531-990 Curitiba, Paraná, Brazil

ABSTRACT: The effect of an external electric field on the formation of protein GlnB-Hs films and on its buffer solution on siliconized glass slides has been analyzed by current versus electric field curves and atomic force microscopy (AFM). The *Herbaspirillum seropedicae* GlnB protein (GlnB-Hs) is a globular, soluble homotrimer (36 kDa) with its 3-D structure previously determined. Concentrations of 10 nM native denatured GlnB-Hs protein were deposited on siliconized glass slides under ambient conditions. Immediately after solution deposition a maximum electric field of 30 kV/m was applied with rates of 3 V/s. The measured currents were surface currents and were analyzed as transport current. Electric current started to flow only after a minimum electric field (critical value) for the systems analyzed. The AFM images showed films with a high degree of directional organization only when the proteins were present in the solution. These results showed that the applied electric field favored directional organization of the protein GlnB-Hs films and may contribute to understand the formation of protein films under applied electric fields.



1. INTRODUCTION

Protein biofilms are essential for human welfare as well as the development of nanotechnology. In addition, protein biofilms can occur naturally or be synthesized. For instance, naturally occurring biofilm formation is essential to the oral microbiota to adhere to the teeth surface.^{1,2} The homeostasis of this biofilm is essential for host protection against dental cavities and periodontal pathologies.^{1–3} Synthetically, protein biofilms have been used for biochips, biomaterials, development of biosensors, implants, microarrays, and bidimensional crystallization, which facilitates the nucleation and growth of protein crystals used in crystallographic studies.^{4–6} Therefore, scrutinizing the kinetics of supramolecular structure formation will shed light into the mechanisms in which organic biofilm is formed and may help design advanced biosensor, biochips, bioelectronics, and a range of medical devices.^{7–13}

Several theoretical as well as empirical approaches have been developed to understand the formation of supramolecular structures, particularly such as protein biofilms onto solid surfaces.^{14,15} For example, electrorheology (ER) is a method that can control solid particles dispersed in an insulating liquid's flow upon the application of an electric field. This occurs due to the charge dependency on buffer characteristics that provides the distinct electrical properties of the macromolecules. The magnitude of the electric field determines the movement of the proteins toward or away from the high-field region. Furthermore, it might generate a local gradient field capable of inducing dipole–dipole interactions between proteins. Thus, ER can be used to control the spatial homogeneity, orientation,

and protein layer growth ratio of a thin biofilm^{13,16} which is ideal for bioparticles manipulation such as stretching, aligning, and transport.^{13,16,17}

Previous work investigated protein adsorption on solid surfaces under an electric field using one of the electrodes as a substrate for film grow and measured layer length,¹⁸ molecule orientation,¹⁹ and antigen–antibody binding.²⁰

In this study, we used external electric field (EEF) for the formation of highly organized thin protein film onto siliconized glass. Siliconized glass has an apolar surface because the main chain of the silicone is Si–O. The silicone is a dielectric polymer with high polarizability when in electric fields of 3 kV/mm,^{21,22} which can aid the orientation of particles. We used native and denatured GlnB of *Herbaspirillum seropedicae* (GlnB-Hs). GlnB-Hs is a signal-transducing protein, which likely signalizes carbon, nitrogen and energy levels to the diazotrophic organism, *H. seropedicae*.²³ It is a globular and soluble trimeric protein of 36 kDa with 3D structure determined at a resolution of 2.1 Å. Structurally, GlnB-Hs has negative charge on the top and bottom faces of the trimeric complex and positively charge on the lateral sides.²³

GlnB-Hs protein films were previously analyzed with atomic force microscopy (AFM) and XPS spectroscopy in different hydrophobics substrates and in different kinds of procedures.^{24,25} The supramolecular structures formed by protein

Received: May 27, 2015

Revised: August 2, 2015

Published: August 31, 2015

GlnB-Hs are dependent on buffer solution and deposition method. Ferreira et al.²⁴ showed that the self-organized protein changed with salt concentration onto bare mica and possible artifacts due to salt contribution. Thin films of GlnB-Hs protein formed on hydrophilic and hydrophobic silicon (1 1 1) and (1 0 0) surface were investigated by AFM and XPS by Lubambo et al.,²⁵ showing self-organization doughnut-like structures on hydrophilic silicon surface and in filaments on hydrophobic Si surface.²⁵

The structure of the biofilms was analyzed through atomic force microscopy (AFM) to verify the organization of the supramolecular structures, and “current against electric field” (*I*–*E*) curves were obtained to determine parameters of reproducibility of those biofilms. We expected to obtain organized structures of protein GlnB-Hs on siliconized glass slide by applying a DC external electric field that can help understand the protein film formation and verify if these supramolecular structures can contribute to the 2D protein crystallization.

2. EXPERIMENTAL METHODS

2.1. GlnB-Hs Protein Solution. The GlnB-Hs protein was purified as described by Benelli et al.;²³ the native protein solution of 50 mM Tris-HCl pH 8, 50 mM NaCl, 0.1 mM EDTA, and 50% glycerol²³ was diluted to final concentration of 0.3 mg/ μ L (10 nM in 50 mM Tris-HCl pH 8, 50 mM NaCl).

GlnB-Hs was denatured by heating the protein solution to 100 °C for 15 min.

2.2. Silicone Microchannels on Siliconized Glass. The rectangular channels were fabricated on glass-siliconized slides (Hampton Research HR 3-231). The channel of silicone paste (polisiloxane) (Sikasil S.A.) walls was designed through a rigid mask of 0.40 ± 0.01 mm wide and 4 ± 0.5 mm long. After the silicone paste dried, the rigid mask was removed. The channel’s depth was about 0.43 ± 0.01 mm. The extremities of the glass-siliconized slide were painted with conductive graphite ink for electrodes so that the electric current applied over the microchannel could be conducted through the material. The protein solutions were deposited between the electrodes filling the microchannel.

2.3. Current Monitoring. The experimental setup system can be seen as an electric circuit composed of resistors connected in series with a parallel plate capacitor with solution deposited between carbon electrodes, as shown in Figure 1. The two resistors of $43.7\text{ k}\Omega$ (resistor 1) and $8.37\text{ k}\Omega$ (resistor 2) connected in series were to avoid short circuit and control the well-functioning of the system.

Immediately after depositing the protein solutions in the silicone microchannel, an electrical potential difference of 0–300 V was applied with a high-voltage power supply (Agilent

Technologies N5752A) and monitored using a Keithley multimeter. Current data were collected and recorded as a function of time using LabView software (National Instruments, TX). The change in the current was detected by measuring the voltage drop (*V*) across the resistor 1, calculated using Ohm’s law for resistors connected in series.²⁶ The voltage was applied in a stepwise manner following increments of 0.75 kV/m·s, starting at 0 V and heading up to 300 V.

The current saturation was established when ions generated by dissociation were quickly neutralized by charge injection from the electrodes. The change in the ions concentration near the electrodes and charge injection in the solution was considered to be responsible for the current saturation or slight continuous increase with larger applied electric fields. To make sure that the artifacts were due to buffer compounds and the substrate, a glass slide covered with an organosilane with surface resistivity of $10^{13}\text{ }\Omega/\text{m}$ (data provided by Hampton Research) was avoided. Control analyses were performed by applying 75 kV/m on a recently deposited buffer solution (50 mM NaCl, 50 mM Tris-HCl pH 8) and on the bare substrate.

2.4. Atomic Force Microscopy. All images were obtained in tapping mode with a commercial AFM (Shimadzu SPM9500J3) equipped with a $30\text{ }\mu\text{m}$ scanner. Silicon cantilevers with spring constant of 42 N/m, resonance frequency of ~ 320 kHz (Nanosensor), and radius tip of 10 nm were used. AFM images of 256×256 pixels were obtained at scan rate of 1.5 Hz in the same direction of the applied electric field. Capturing AFM images in the same direction of the applied EEF (external electric field) allowed us to control the position of the tip of the microscope, which was, consequently, aligned with the applied electric field. All of the measurements were conducted at ambient humidity (40–70%). The samples were prepared in triplicate, and six random regions of 5 to $1.25\text{ }\mu\text{m}$ within each sample were chosen for analysis. By capturing six random regions within each one, we expected to have an accurate description of the structure of the film.

3. RESULTS AND DISCUSSION

3.1. Electric-Field Effects on Native GlnB-Hs Protein Films Formed on Silicone Channels. In previous experiments, native GlnB-Hs protein solution when dispensed directly onto solid surfaces by drop deposition showed self-organization in doughnut-like structures, for both bare mica²⁴ and hydrophilic silicon surface, contrasting with filamentary structures formed on hydrophobic Si surface.²⁵ Similarly, films of native GlnB-Hs formed by drop deposition on siliconized glass slides also formed doughnut-like supramolecular structures (132 ± 18 nm wide), indicated by arrows in the Figure 2A, which were randomly distributed on the surface.

Otherwise, the thin film formed by native GlnB-Hs solution exposed to the external electric field completely covers the siliconized glass area analyzed (Figure 2B), showing holes of 50 ± 10 nm on the organized structures aligned along the external electric field lines. This shows that the electric field rearranged the supramolecular structures during the formation of high organized protein thin films.

Ferreira et al.²⁴ showed that buffer compounds also formed globular supramolecular structures on mica when deposited by drop deposition.²⁴ These globular shapes can induce misleading interpretation of AFM images due to the similarities between the structures formed by buffer compounds and those of protein origin (Figure 3).

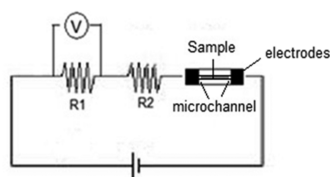


Figure 1. Schematic of electric circuit for current monitoring. The silicon microchannel filled with solution was connected to two resistors, R1 and R2, assembled in series. The change in the current was detected by measuring the voltage drop (*V*) across the first resistor, R1. The data were collected with LabView program.

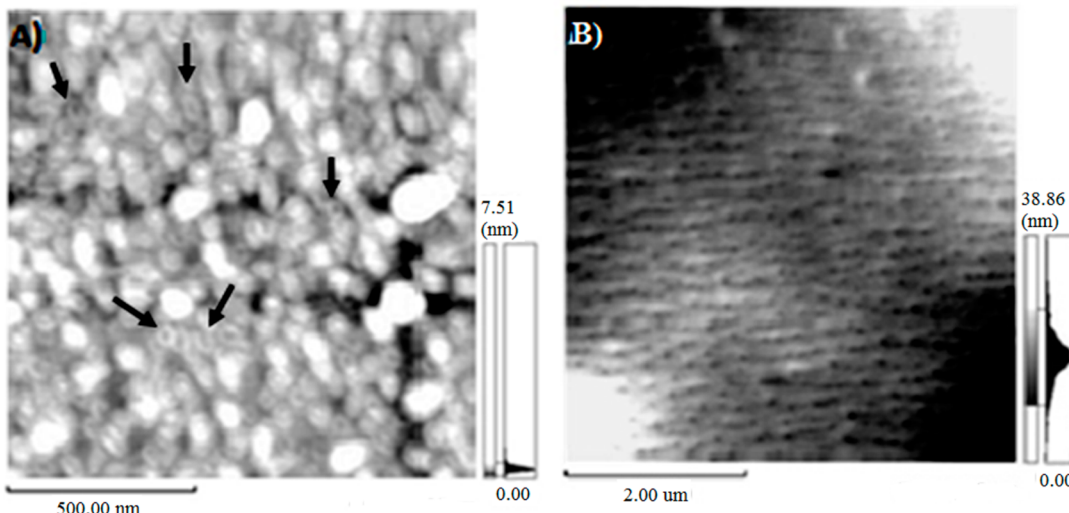


Figure 2. AFM topography images of films onto siliconized glass slides formed by (A) native GlnB-Hs protein films formed by drop deposition with zero electric field (the arrows point to some of the doughnut-like supramolecular structures) and (B) native GlnB-Hs protein film formed after exposition to the external electric field, showing that the organized structures aligned along the external electric field lines.

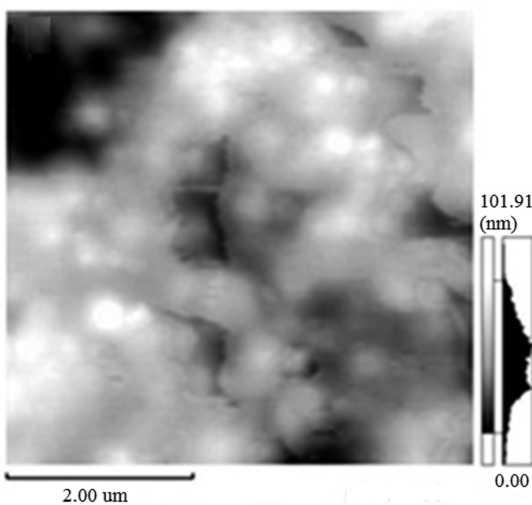


Figure 3. AFM topographical image control of thin film on siliconized glass slides formed by buffer solution (50 mM NaCl, 50 mM Tris-HCl pH8) exposed to the external electric field, in which aggregates randomly distributed in a misshape pattern are observed.

The result of the buffer solution showed that the film formed does not present any evidence of orientation due to the applied electric field, showing only aggregates randomly distributed in a misshape pattern (Figure 3), leading to no dubious interpretation when compared with protein films. Indeed, the lack of orientation evidence of the film of the buffer solution submitted to an electric field could be associated with the absence of large polar molecules, like proteins, that keep orientation along the field lines.

3.2. Electric Field Effects on Denatured GlnB-Hs Protein Films Formed on Silicone Channels. When the denatured GlnB-Hs protein solution was dispensed directly onto the siliconized surface, the AFM images showed self-organized supramolecular structures randomly distributed, with evidence of superposition over the substrate (Figure 4A), similarly to the native protein film (Figure 2A). In the case of denatured GlnB-Hs protein, a pattern of fibrous-like discon-

tinued film was formed, containing pellets, of 163 ± 39 nm wide (Figure 4A).

Conversely, the film formed by denatured GlnB-Hs solution under 75 kV/m of EEF displayed aligned filaments of 166 ± 33 nm diameter and $>5 \mu\text{m}$ length, covering the whole surface of the substrate that was analyzed (Figure 4B).

The denatured GlnB-Hs protein orientation, observed in Figure 4B, is due to polarization orientation, to the gradient field, and to the influence of the counterion cloud surrounding the biomolecules. This was explained before by Washizu et al.,²⁸ in which DNA molecules in high-frequency high-intensity field became polarized and the electrostatic orientation aligned every part of DNA parallel to the field. The polarized charges are pulled toward the electrodes by dielectrophoresis; finally, the molecules are aligned onto the electrodes.²⁸

The application of an electric-field-induced orientation of the polarized molecular dipoles and a colloid flow was determined by electrorheological (ER) effects.^{13,16,17} The particles in an ER fluids subjected to a uniform electric field align in the direction of the electric field, forming first chains and then columns as two or more chains merge together.^{12,16,27}

The behavior of the proteins solution under the external electric field can be explained by the interactions between the applied field with molecular dipoles; induced dipole with local dipole, and local dipole–dipole interactions, all constrained by interfaces air–liquid and liquid–solid substrates. When an electric field is applied to the protein solutions spread onto a solid surface, the molecules became polarized and may be displaced by the gradient of local fields, owing to the difference in the dielectric constant of the macromolecules and that of the solvent.¹⁶ For molecular dipoles, the polarization is the result of competition between the alignment energy $-\vec{p}_0 \cdot \vec{E} = -p_0 E \cos \theta$ and thermal Brownian motion, where θ denotes the angle between the electric field and the molecular dipole moment p_0 .^{13,16} In general, the polarization may arise from various mechanisms of charge transport, such as orientation of atomic or molecular dipoles and interfacial polarization.²⁷ Under the electric field E , the particles become polarized (indicated by the arrows in Figure 5) and may be displaced due to the gradient caused by the difference in dielectric constant between the

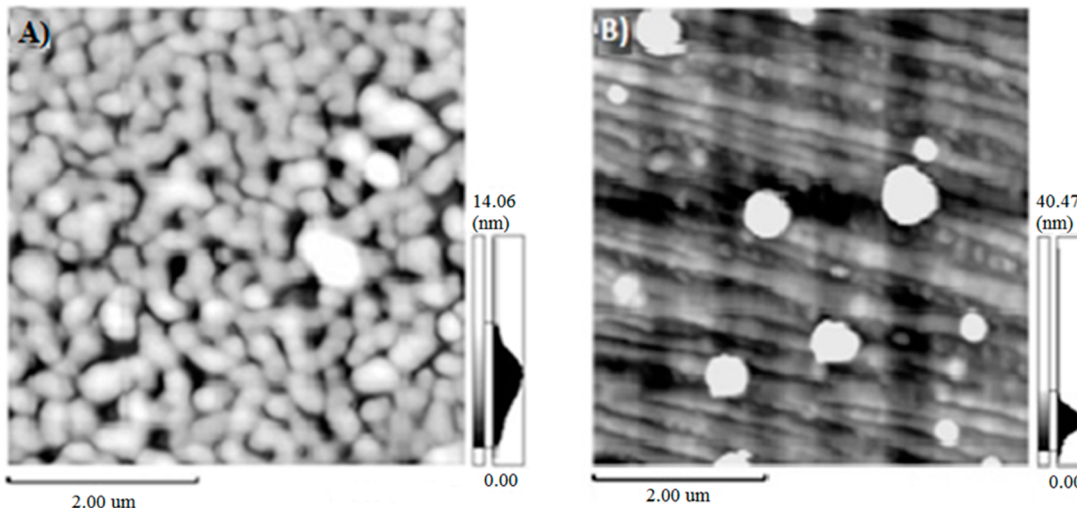


Figure 4. AFM topography images of films onto siliconized glass slides formed by (A) denatured GlnB-Hs protein film formed by drop deposition with zero electric field (self-organized supramolecular structures randomly distributed form a pattern of fibrous-like discontinued film) and (B) denatured GlnB-Hs solution exposed to the external electric field, displaying aligned filaments that cover the whole surface of the substrate that was analyzed.

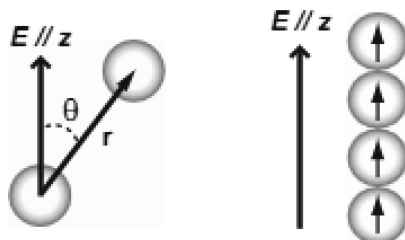


Figure 5. Dipole–dipole interaction induced by an electric field.¹⁹ The electrostatic forces between the particles lead to aggregates that are aligned in the direction of the applied field.

particle material and carrier fluid. For each pair of particles the vector \mathbf{r} , which connects their centers, forms an angle θ with the direction of the external electric field, oriented along the z axis (Figure 5). The dipoles (depicted as arrows) favor particle

configurations in which they are displaced to be aligned in a fashion that minimizes the energy system.¹⁹

The resulting dipole–dipole interaction between the components of the solution tend to form chains along the applied field lines.^{16,27} Therefore, the stable chains observed in Figures 2B and 4B follow the same trend as simulations of nanosized particles of dielectric suspensions.¹² Kadaksham et al.¹² used direct numerical simulation of dielectric suspensions subjected to uniform electric field for nanosized particles to study the influence of Brownian forces on the particle structure formation. They showed that in a uniform electric field with rigid particles of 200 nm diameter and 1.01 g/cm³ in a domain of size 1.5 and 3.36 μm³ when the parameter that measured the ratio of dipole force to the Brownian force was 100 or larger, particles come together to form a pearl-chain parallel to the electric field because the Brownian force was not sufficiently

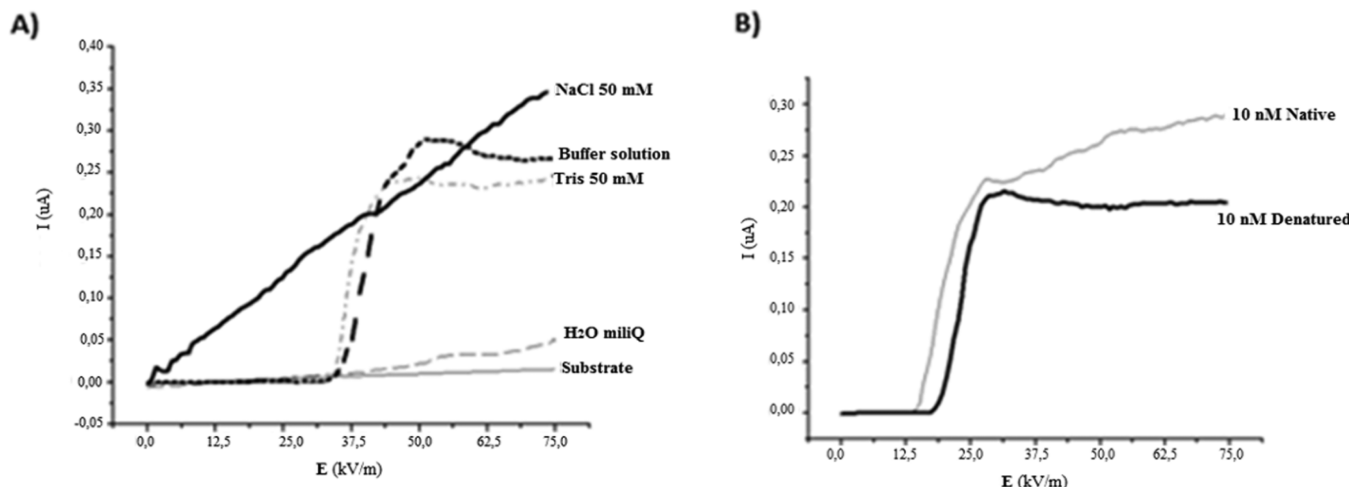


Figure 6. Curves $I-E$ of (A) controls solutions: H₂O Milli-Q (dashed curve), 50 mM Tris (dashed-dotted curve), 50 mM NaCl (black curve), buffer solution (50 mM NaCl, 50 mM Tris-HCl pH 8) (dashed black curve), and the empty channel (silicone substrate) (light-black curve) and (B) native (light-black curve) and denatured (black curve) 10 nM GlnB-Hs protein solutions. The critical E_c value was determined by the minimal electric field required for sharp current increase, and above this critical E_c value corresponding to dissociation of ions the saturation region was reached due to equilibrium between ion dissociations and electron/hole injection.

strong to overcome the particle–particle interaction force.¹² The numerical simulation used was a generalization of the Distributed Lagrange Multiplier method (DLM) finite element, well described in Glowinski,²⁹ where they varied the ratio of the electrostatic particle–particle interaction and the uniformity of the field and the Brownian force, showing the dependence of the particle scale structure evolution on the Brownian forces.¹²

Our AFM images, Figures 2B and 4B, show evidence that the particle–particle electrostatic interaction force and hydrodynamic force overcomes the Brownian motion when the external electric field is quickly increased up to a critical value E_c (discussed in the next section). The pearl chain of spherical particles illustrated in Figure 5 and explained by Kadaksham et al.¹² is an oversimplified model to explain the alignment of nature and denature proteins, especially because proteins have different polar groups and are deformable macromolecules that may deform along the electric field lines favoring further alignment; however, Kadaksham et al.¹² is an excellent basic approach to understand the basis of the dielectrophoretic forces acting in the system that are even more complex.

3.3. I–E Curves. The control I – E curves for the siliconized glass showed negligible flow through the channel (Figure 6A). Therefore, when a voltage V was applied across the electrodes, the current I flowed mainly through the solution filling the channel. The capacitive energy stored was negligible because the capacitor cross section was quite small and the distance between electrodes was large, so that the capacitance of the channel was on the order of a few picofaraday. As a result, the total current was mostly equal to the flow of the free charged particles and the drag of proteins and others macromolecules in solution.

Because of the external electric field, charges are redistributed at the interface of the electrode and through the solution to compensate for the external distortion, forming an electrostatic shield. This leads to the formation of the electric double layer at the interface electrode–solution¹⁷ and polarization of some species. These changes in the ions/molecules distribution in the solution affect the electrical current because they depend on carriers number and particles mobility. Therefore, current density flowing through the solution depends on the conductivity of the solvent and the local electric field.³⁰ It is worth recalling that in addition to the complexity of the aqueous solution there were two interfaces that interfere with the effective conductivity, the solution–air, and solution–solid.

I – E curves consist of three regions: capacitor charging, dissociation, and saturation (Figure 6). For solutions of Tris-HCl, buffer, and proteins, the current was negligible until a critical electric field (E_c) was reached (Table 1). The critical E_c value was determined by the minimal electric field required for sharp current increase. Above this critical E_c value, correspond-

ing to dissociation of ions (H^+ , OH^- , Na^+ , Cl^-) released from solvation layers of polar compounds and GlnB-Hs protein, the saturation region was reached due to equilibrium between ion dissociations and electron/hole injection. The nonlinearity in the current–voltage characteristics is well-defined for micro-nanochannel integrated system^{17,31–33} and bipolar membranes.³⁴ Furthermore, as expected, we found that NaCl solution behaves as an ionic solution with linear current–voltage curves (Figure 6A).

The currents measured (Figure 6) were due to different types of mass-transfer phenomena for the ionic species in electrolytes near the electrodes:³⁵ (1) diffusional transport under concentration gradients, (2) migration of oppositely charged ions under electric field of the electrodes, and (3) convection transport due to physical stirring of the electrolyte, which can be neglected in the case of thin films; however, ionic current transport could induce considerable forces on electrolytes in nanometer-size particles, as a result of which convection has to be considered.^{17,35} Concentration polarization does occur under these conditions as well as a complex set of effects related to the formation of ionic concentration gradients in the electrolyte solution adjacent to an ion-selective interface.^{17,35} The control curves (Figure 6A) of 50 mM Tris-HCl and buffer solution have similar characteristics for the critical E_c value of 34 kV/m; however, the saturation current for the buffer solution was higher (Table 1). After a small decrease in the current value to 0.27 μ A, the current saturates for buffer solution. For H₂O Milli-Q, the critical E_c value was negligible (Table 1), followed by a slow current increase.

Tris-HCl pH 8 and buffer solutions (Figure 6A) presented negligible current flow below their corresponding critical field (Table 1) due to low charge availability in the fluid to constitute ionic current. Tris molecule is an organic compound known as tris(hydroxymethyl)aminomethane [(HOCH₂)₃CNH₂], with pK_a of 8.06 at 25 °C. In the presence of the applied electric field, these molecules will suffer low electrostatic force due to dissociation equilibrium until the critical value E_c of 34 kV/m was reached. Higher fields imply on ionic dissociation, resulting in a quick increase in the current (see Table 1) up to saturation.

Depending on the polarity of the applied electric field, the uneven ions flows from the two ends lead to either accumulation or depletion of ions in the channel and, as a result, either enhancement or reduction of the ionic conductance.³⁶ When protein was added in the solutions (Figure 6B), the curves showed negligible current until the critical E_c values of 14 kV/m for native GlnB-Hs and 17 kV/m for the denatured GlnB-Hs. The current then increases rapidly with the applied electric field until saturation (Figure 6B and Table 1). In the case of native GlnB-Hs, after the saturation there was a slight decrease, followed by a smooth increase. For the denatured GlnB-Hs, the current gradually reached a limiting value that remains constant with further E increase.

The channel filled with Tris-HCl pH 8 generates charged species such as Tris neutral with its protonated form, ions Cl^- and OH^- and H_3O^+ due the protolysis reaction of water molecules,³⁷ and Na^+ and Cl^- in saline solution in a stable, neutral, and uniform distribution. The presence of protein, in proximity to its isoelectric point, trapped enough ions to neutralize its polar nature. Charge carriers in liquids were electrons, holes, and ions;^{38,39} however, there are many situations where free electrons in liquids are quickly trapped

Table 1. I–E Curves for Control and 10 nm Native and Denatured Protein Solutions^a

	solutions	critical E_c value (kV/m)	saturation I (μ A)
controls	H ₂ O Milli-Q	3	0.03
	50 mM Tris	34	0.29
	buffer solution	34	0.23
proteins	10 nM native	14	0.23
	10 nM denatured	17	0.21

^aCritical E value is defined as the electric field just before the current starts to increase.

by electronegative impurities or molecules of the liquid. In most cases, the charge carriers in liquids will be ions in dissolution.³⁸

The presence of native and denatured GlnB-Hs protein in the buffer solution drastically drops the critical value of the electric field (E_c) (Figure 6B). The presence of the protein in the solution causes a redistribution of the diffuse charge around the polarized macromolecules due to the dissociation field effect, leading to a shift of its surface potential.^{40,41} Then, the stabilization of dissociated and the water molecules around the macromolecules does not have sufficient time to trap and neutralize the ions before the migration transport occurs.⁴¹ The net result is that the conductivity of the solution increases, and this is called the Wien effect.^{41,42}

On the basis of the classical assumptions of concentration polarization, the limiting current could not be exceeded unless ions other than salt ions became available for current transport in the salt-depleted double layer. This was the case when water dissociation leads to the production of H^+ and OH^- ions, which will then carry the electric charges, resulting in so-called overlimited currents. As a consequence, pH value shifts are obtained, with increasing pH values on the anodic side of the nanochannel and decreasing pH values on the cathodic side.¹⁷

The AFM images showed supramolecular structures aligned with the field lines and the critical E_c value was drastically smaller only when GlnB-Hs protein was present in buffer solution. Indeed, the lack of orientation evidence of the solution of films submitted to an electric field can be associated with the absence of large molecules, like proteins, that keep orientation along the field lines. The advantage of using E is the sensitivity for low amounts of biomolecule regarding buffer compounds concentration.

4. CONCLUSIONS

Electrorheological properties were used to obtain oriented thin protein films by organized native and denatured GlnB-Hs supramolecular structures on glass-siliconized surface with a simple setup system.

The AFM topographical images can be used to evidence the presence of proteins in the solution. The aligned supramolecular structures, even for a small concentration of GlnB-Hs, were formed only in the presence of proteins.

$I-E$ curves showed that a minimal electric-field value was necessary for current to be measured due to the dissociation of the solution compounds formed between buffer and the GlnB-Hs proteins inside the channel. The presence and protein tridimensional structure alters the critical E value for current flow.

These results can contribute to the advance of former alignment supramolecular structures, such as extended biomolecules being used as a base for organization and assembly of molecules or nanoparticles on a solid substrate, for example, in protein bidimensional crystallization and construction of molecular electronic devices.

■ AUTHOR INFORMATION

Corresponding Author

*Phone/Fax: +55 (41) 3361-3308. E-mail: fabi_ferreira@ymail.com.

Present Address

¹P.C.C.: DF, Federal University of São Carlos, Rodovia Washington Luís, Km 235, s/n - Jardim Guanabara, São Carlos 13565-905, São Paulo, Brazil.

Notes

The authors declare no competing financial interest.

■ ACKNOWLEDGMENTS

We thank Juliano Morimoto for comments on the original versions of the manuscript, Ivo Hummelgen for laboratory and equipment use, and CNPq for financial support.

■ REFERENCES

- (1) Avila, M.; Ojcius, D. M.; Yilmaz, O. The Oral Microbiota: Living with a Permanent Guest. *DNA Cell Biol.* **2009**, *28*, 405–411.
- (2) Hannig, C.; Hannig, M. The Oral Cavity – a Key System to Understand Substratum-Dependent Bioadhesion on solid Surfaces in Man. *Clin Oral Invest.* **2009**, *13*, 123–139.
- (3) Colombo, A. P. V.; do Souto, R. M.; da Silva-Bogossian, C. M.; Miranda, R.; Lourenço, T. G. B. Microbiology of Oral Biofilm-Dependent Diseases: Have We Made Significant Progress to Understand and Treat These Diseases? *Curr. Oral Health Rep.* **2015**, *2*, 37–47.
- (4) Pechkova, E.; Nicolini, C. Protein Nanocrystallography: a New Approach to Structural Proteomics. *Trends Biotechnol.* **2004**, *22*, 117–122.
- (5) Malkin, A.; Kuznetsov, Y.; McPherson, A. In situ Atomic Force Microscopy Studies of Surface Morphology, Growth Kinetics, Defect Structure and Dissolution in Macromolecular Crystallization. *J. Cryst. Growth* **1999**, *196*, 471–488.
- (6) Astier, J.; Bokern, D.; Lapena, L.; Veesler, S. α -Amylase Crystal Growth Investigated by in situ Atomic Force Microscopy. *J. Cryst. Growth* **2001**, *226*, 294–302.
- (7) Lowe, C. R. Nanobiotechnology: The Fabrication and Applications of Chemical and Biological Nanostructures. *Curr. Opin. Struct. Biol.* **2000**, *10*, 428–434.
- (8) Hlady, V.; Buijs, J. Protein Adsorption on Solid Surfaces. *Curr. Opin. Biotechnol.* **1996**, *7*, 72–77.
- (9) Gray, J. The Interaction of Proteins with Solid Surfaces. *Curr. Opin. Struct. Biol.* **2004**, *14*, 110–115.
- (10) Zhu, H.; Snyder, M. Protein Chip Technology. *Curr. Opin. Chem. Biol.* **2003**, *7*, 55–63.
- (11) Rabe, M.; Verdes, D.; Seeger, S. Understanding Protein Adsorption Phenomena at Solid Surfaces. *Adv. Colloid Interface Sci.* **2011**, *162*, 87–106.
- (12) Kadaksham, A.; Singh, P.; Aubry, N. Dielectrophoresis of Nanoparticles. *Electrophoresis* **2004**, *25*, 3625–3632.
- (13) Wen, W.; Huang, X.; Sheng, P. Electrorheological Fluids: Structures and Mechanisms. *Soft Matter* **2008**, *4*, 200–210.
- (14) Rabe, M.; Verdes, D.; Zimmermann, J.; Seeger, S. Surface Organization and Cooperativity during Nonspecific Protein Adsorption Events. *J. Phys. Chem. B* **2008**, *112*, 13971–13980.
- (15) Andrade, J.; Hlady, V.; Wei, A. Adsorption of Complex Proteins at Interfaces. *Pure Appl. Chem.* **1992**, *64*, 1777–1781.
- (16) Sheng, P.; Wen, W. Electroheological Fluids: Mechanisms, Dynamics and Microfluids Applications. *Annu. Rev. Fluid Mech.* **2012**, *44*, 143–174.
- (17) Schoch, R.; Han, J.; Renaud, P. Transport Phenomena in Nanofluidics. *Rev. Mod. Phys.* **2008**, *80*, 839–883.
- (18) Brusatori, M. A.; tie, Y.; Van Tassel, P. R. Protein Adsorption Kinetics under an Applied Electric Field: An Optical Waveguide Lightmode Spectroscopy Study. *Langmuir* **2003**, *19*, 5089–5097.
- (19) Leunissen, M. E.; Sullivan, M. T.; Chaikin, P. M.; van Blaaderen, A. Concentrating Colloids with Electric Field Gradients I. Particle Transport and Growth Mechanism of Hard-Sphere-Like Crystals in an Electric Bottle. *J. Chem. Phys.* **2008**, *128*, 164508–164511.
- (20) Kirby, B. J. *Micro- and Nanoscale Fluid Mechanics: Transport in Microfluidic Devices*; Cambridge University Press: New York, 2010.
- (21) Xia, H.; Takasaki, M.; Hirai, T. Actuation Mechanism of Plasticized PVC by Electric Field. *Sens. Actuators, A* **2010**, *157*, 307–312.

- (22) Klykken, P.; Servinski, M.; Thomas, X. *Silicone Film-Forming Technologies for Health Care Applications*; Corning Corporation, 2009.
- (23) Benelli, E.; Souza, E.; Funayama, S.; Rigo, L.; Pedrosa, F. Evidence for Two Possible glnB-type Genes in *Herbaspirillum seropedicae*. *J. Bacteriol.* **1997**, *179*, 4623–4626.
- (24) Ferreira, C. F. G.; Benelli, E.; Klein, J. J.; Schreiner, W.; Camargo, P. C. Effect of Protein Solution Components in the Adsorption of *Herbaspirillum seropedicae* GlnB Protein on Mica. *Colloids Surf., B* **2009**, *73*, 289–293.
- (25) Lubambo, A.; Benelli, E.; Klein, J.; Schreiner, W.; Camargo, P. X-Ray Study of *Herbaspirillum Seropedicae* GlnB Protein Adsorbed on Silicon. *Cell Biochem. Biophys.* **2006**, *44*, 503–511.
- (26) Tipler, P. A.; Mosca, G. *Physics for Scientists and Engineers*; W.H. Freeman and Company: New York, 2008; pp 145–190.
- (27) See, H. Advances in Modeling the Mechanisms and Rheology of Electrorheological Fluids. *Korea-Aust. Rheol. J.* **1999**, *11*, 169–195.
- (28) Suzuki, S.; Yamanashi, T.; Tazawa, S.; Kurosawa, O.; Washizu, M. Quantitative Analysis of DNA Orientation in Stationary AC Electric-Fields Using Fluorescence Anisotropy. *IEEE Trans. Ind. Appl.* **1998**, *34*, 75–83.
- (29) Glowinski, R. T.; Pan, W.; Hesla, T. I.; Joseph, D. D. A Distributed Lagrange Multiplier/Fictitious Domain Method for Particulate Flows. *Int. J. Multiphase Flows* **1998**, *25*, 755–794.
- (30) Tian, Y.; Wen, S.; Meng, Y. Conductivity Effect in Electrorheological Fluids. *Sci. China, Ser. G: Phys., Mech. Astron.* **2004**, *47*, 59–64.
- (31) Kim, S.; Wang, Y.; Lee, J.; Jang, H.; Han, J. Concentration Polarization and Nonlinear Electrokinetic Flow near a Nanofluidic Channel. *Phys. Rev. Lett.* **2007**, *99*, 044501.
- (32) Yossifon, G.; Chang, H. Selection of Nonequilibrium Over-limiting Currents: Universal Depletion Layer Formation Dynamics and Vortex Instability. *Phys. Rev. Lett.* **2008**, *101*, 254501.
- (33) Yossifon, G.; Mushenheim, P.; Chang, Y.; Chang, H. Nonlinear Current-Voltage Characteristics of Nano-Channels. *Phys. Rev.* **2009**, *79*, 046305.
- (34) Song, J.; Yeon, K.; Moon, S. Effect of Current Density on Ionic Transport and Water Dissociation Phenomena in a Continuous Electrodeionization (CEDI). *J. Membr. Sci.* **2007**, *291*, 165–171.
- (35) Vyasa, R.; Wang, B. Electrochemical Analysis of Conducting Polymer Thin Films. *Int. J. Mol. Sci.* **2010**, *11*, 1956–1972.
- (36) Cheng, L.; Guo, L. Ionic Current Rectification, Breakdown, and Switching in Heterogeneous Oxide Nanofluidic Devices. *ACS Nano* **2009**, *3*, 575–584.
- (37) Hlushkou, D.; Perdue, R.; Dhopeshwarkar, R.; Crooks, R.; Tallarek, U. Electric Field Gradient Focusing in Microchannels with Embedded Bipolar Electrode. *Lab Chip* **2009**, *9*, 1903–1913.
- (38) Bartnikas, R. *Electrical Insulating Liquids (Engineering Dielectrics)*; ASTM International Press: Philadelphia, PA, 1994; Vol. 3.
- (39) Ryu, J.; Park, H.; Park, J.; Kang, K. New Electrohydrodynamic Flow Caused by the Onsager Effect. *Phys. Rev. Lett.* **2010**, *104*, 104502.
- (40) Kirby, B.; Hasselbrink, E., Jr. Zeta Potential of Microfluidic Substrates: 1. Theory, Experimental Techniques, and Effects on Separations. *Electrophoresis* **2004**, *25*, 187–202.
- (41) Park, J.; Ryu, J.; Kim, W.; Kang, K. Effect of Electric Field on Electrical Conductivity of Dielectric Liquids Mixed with Polar Additives: DC Conductivity. *J. Phys. Chem. B* **2009**, *113*, 12271–12276.
- (42) Morgan, H.; Green, N. *AC Electrokinetics: Colloids and Nanoparticles*; Research Studies Press: Baldock U.K., 2003.